8000-cm^{-1} line spectrum in platinum-doped silicon studied by perturbation spectroscopy

Janos Olajos, Mats Kleverman, and Hermann G. Grimmeiss
Department of Solid State Physics, University of Lund, P.O. Box 118, S-221 00 Lund, Sweden
(Received 17 May 1989)

A thorough investigation by means of perturbation spectroscopy and electron paramagnetic resonance has been carried out on the line spectrum at about 8000 cm^{-1}, recently observed in platinum-doped silicon. The uniaxial stress and Zeeman results show that this center has tetrahedral symmetry. The optical transitions are conclusively identified as excitations to donorlike excited states from a $\Gamma_7(T_2)$ ground state, and substitutional Pt in its singly positively charged state is suggested as the center's chemical origin.

I. INTRODUCTION

Platinum-related centers in silicon have been extensively studied over the years, in particular the biaxial-Pt center which was observed already in the early 1960's in the electron paramagnetic resonance (EPR) experiments by Ludwig and Woodbury.[1] This center has been identified as the isolated negatively charged substitutional center (Pt^-) showing C_{2v} point-group symmetry consistent with a superposition of tetragonal and trigonal distortions. The similarities between the electronic properties of Pt^- and the well-established properties of the monovacancy in silicon resulted in the vacancy model[2] for the platunim center. This model assumes that platinum in a closed-shell configuration, $5d^{10}$, enters a vacancy and the electronic properties are essentially similar to the vacancy. Pt^- has also been studied by means of different junction space-charge techniques from which the activation energies for transitions between different charge states have been determined. The levels in the band gap are $E_v+0.32$ meV ($Pt^0 \rightarrow Pt^+$) and $E_c-0.23$ meV ($Pt^0 \rightarrow Pt^-$) (Ref. 3); the acceptor level being found above the donor level in the band gap, which is also the case for gold[4] in silicon. Sharp-line spectra have recently been observed in platinum-doped silicon using different techniques, e.g., photoluminescence,[5] absorption,[6] and photothermal ionization spectroscopy[7] (PTIS). A typical transmission spectrum is presented in Fig. 1. The transitions at photon energies in the range 7380 to 7800 cm^{-1} have been conclusively ascribed to the isolated Pt center by a combination of experimental results obtained by photo EPR and by PTIS.[8] These lines have their origin in bound-to-bound hole transitions from the deep ground state to delocalized shallow excited hole states at the neutral isolated Pt center (Pt^0).

The already mentioned PTIS study reported on the observation of a new Pt-related line spectrum. The spectrum consists of three sharp lines at about 8000 cm^1, which were labeled T_1, T_2, and T_3 (see Fig. 1). No information on the origin of these T lines could be established, but it was convincingly demonstrated that the T lines did not belong to the acceptor spectrum. Furthermore, the three lines were always observed with the same relative intensity, indicating that they have a common origin, and it was also found that, for a specific shallow-dopant concentration of the starting material, their intensity relative to the acceptor lines was similar in different samples.

The total potential seen by a charge carrier bound to a defect in a semiconductor can be divided into two parts. One which is short range, and a second long range, being the well-known screened Coulomb potential. Shallow donor and acceptor states are derived from the bottom of the conduction band and the top of the valence band, respectively, and their wave functions are extended in real space. In the central-cell region, where the localized potential is strong, the amplitude of the wave functions of the p-like states is small and, thus, they are only affected to a minor extent by a central-cell correction. This implies that the p-like states of shallow donors and acceptors in silicon are well described by the effective-mass theory (EMT),[9] which accounts for the energy-level structure caused by the screened Coulomb potential. The shallow states are thus uniquely defined by the semiconductor material only and may serve as a "fingerprint" for the donor or acceptor bound-to-bound transitions. The EMT level scheme has, therefore, been successfully applied to several deep-level spectra in silicon.[10–13] However, the electric-dipole selection rules and intensities depends on the electronic properties of the specific deep

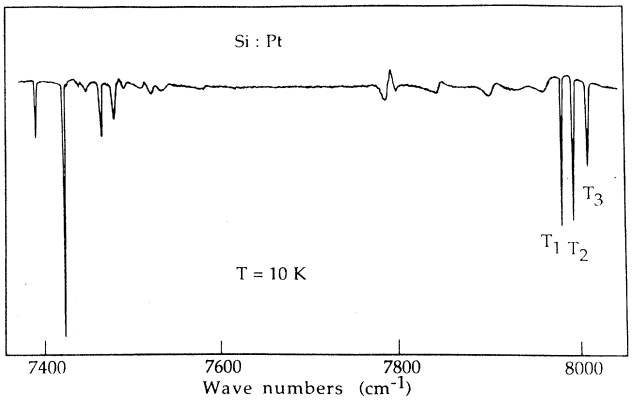

FIG. 1. Transmission spectrum of Pt-doped silicon showing sharp-line spectra due to the acceptor and the T-line center.

 ©1989 The American Physical Society

center, since the localized potential determines the electronic properties of the ground state. Such effects have been observed in the spectra for the deep chalcogen donors in silicon,[10] where an EMT-forbidden (but symmetry allowed) intra-1s transition has comparable intensity to the strongest EMT-allowed transitions. A line spectrum obtained from Ag-doped silicon[12] was interpreted as dominated by EMT-forbidden transitions. This shows that a comparison with shallow-level spectra may give useful information in many cases, but exceptions to the "fingerprint rule" may be expected. In the PTIS work,[7] the T lines were not observed as part of an EMT series, which made an analysis based on line spacings and relative intensities impossible. Furthermore, no electronic continuum was observed, as in the case of the Pt-acceptor spectrum and, hence, no combined photo EPR and PTIS experiments were possible. Thus, the electronic properties and the chemical origin of the T-line center remained unknown.

Perturbation methods in conjunction with, for example, transmission measurements, may give useful information on the electronic properties of defects in semiconductors. Uniaxial-stress spectroscopy has proven to be a valuable tool for studying centers showing orientational and/or electronic degeneracy and may determine their symmetry properties. This method can also be used to bring different states into near resonance, thereby enhancing the coupling between states of equal symmetry and making originally invisible lines visible. An analysis of such stress patterns may establish the symmetry of the center and indicate the labeling of the wave functions, i.e., the irreducible representation and row index of the relevant point group according to which they transform. The fitting parameters of a parametrized theoretical model, may be related to the spin-orbit (s.o.) coupling or the exchange interaction, for example, and the method can therefore be used to determine the strength of such effects.

Stress can only affect the orbital part of the wave functions, leaving half-integer spin systems at least twofold degenerate due to Kramer's degeneracy. Zeeman spectroscopy is yet another common perturbation method applied to numerous defect problems in semiconductors which enables studies on the spin part of the wave function. This method gives information on certain properties, such as g values and total spin, which are difficult or even impossible to obtain by other methods, in particular, when no EPR signal can be detected. Furthermore, EPR measurements offer information on the ground state only, whereas in Zeeman spectroscopy, both the ground and the excited states are probed.

The purpose of this paper is to report on a detailed study on the platinum-related T lines by means of transmission spectroscopy in combination with uniaxial stress and a magnetic field. The experimental data are fitted to a simple model based on EMT and the deformation-potential approximation (DPA) (Ref. 14) for donor impurities. The excellent agreement between theory and experiment enables a symmetry labeling and an identification of both the initial and final states. A tentative assignment of the chemical origin and the charge state is presented and the possibility of lattice distortions, as previously observed, for Pt^- is discussed. The outline of the paper is as follows. After a presentation of the sample preparation procedures and experimental conditions, preliminary stress results are presented and, to some extent, discussed in order to determine a possible identification of electronic states involved as well as to establish a theoretical model for the experimental data. In the next section of the paper, we present the parametrized theoretical model, followed by a full presentation of the experimental results, which are then discussed in detail. Finally, we conclude and tentatively assign the chemical origin and charge state of the T-line center.

II. EXPERIMENTAL DETAILS

The samples used in this study were prepared by means of solid-state diffusion. High-purity platinum was sputtered onto the surfaces of lapped, polished, and etched ($HF+H_2O$) floating-zone silicon. An x-ray elemental analysis of the thin platinum layer after sputtering showed no contamination by other elements from, for example, the platinum source or the sputtering apparatus. Several diffusion experiments were carried out on different starting materials: phosphorus-doped n type with resistivities of 0.09, 0.15, and 5.0 Ω cm and boron-doped p type with resistivities of 0.6, 3.5, 10, and 14 Ω cm. Sputtering for about 1 h resulted in an approximately 100 nm thick platinum layer. After sputtering, the samples were placed in quartz ampules containing argon gas at about 300 mbar and then sealed. The heat treatment was carried out at a diffusion temperature of about 1260 °C for 6 days, followed by a fast quenching to room temperature in diffusion-pump oil. After orientation by x-ray Laue backscattering, samples were cut in the three main directions $\langle 100 \rangle$, $\langle 110 \rangle$, and $\langle 111 \rangle$ with typical dimensions of about $2\times2\times6$ mm^3 for the uniaxial stress experiments and about $8\times5\times3$ mm^3 for the Zeeman experiments. The dimensions were measured using a micrometer screw. Different optical filters and polarizers were used when necessary.

In the case of samples for uniaxial stress experiments, the end surfaces were lapped parallel and the uniaxial stress was applied to the samples by a pneumatic cylinder via a pushrod made of stainless steel. The magnitude of the stress was calculated from the gas pressure in the cylinder and the sample area. In the transmission experiments, the sample temperature was kept at about 10 K in a Leybold continuous-flow cryostat using liquid helium as a coolant.

In the Zeeman experiments, an Oxford Instruments superconducting split-coil spectromagnet was used in the Voigt configuration. The maximum magnetic field was 6.5 T. The sample temperature was accurately controlled in the range 1.6–30 K with a temperature-control unit. All spectra were recorded with a Bomen DA3 02 Fourier-transform infrared spectrometer equipped with a liquid-nitrogen-cooled InSb photodiode detector.

III. REMARKS ON PRELIMINARY RESULTS

In order to establish the conditions for a maximum absorption signal due to the T lines, several diffusion experiments were carried out. In our case, the highest intensity was found using 0.6 Ω cm p-type material for the diffusion conditions presented above. In these samples, the acceptor lines were almost invisible. The uniaxial-stress behavior of the T lines, for stress parallel to the three main directions, is presented in Fig. 2. It is notable

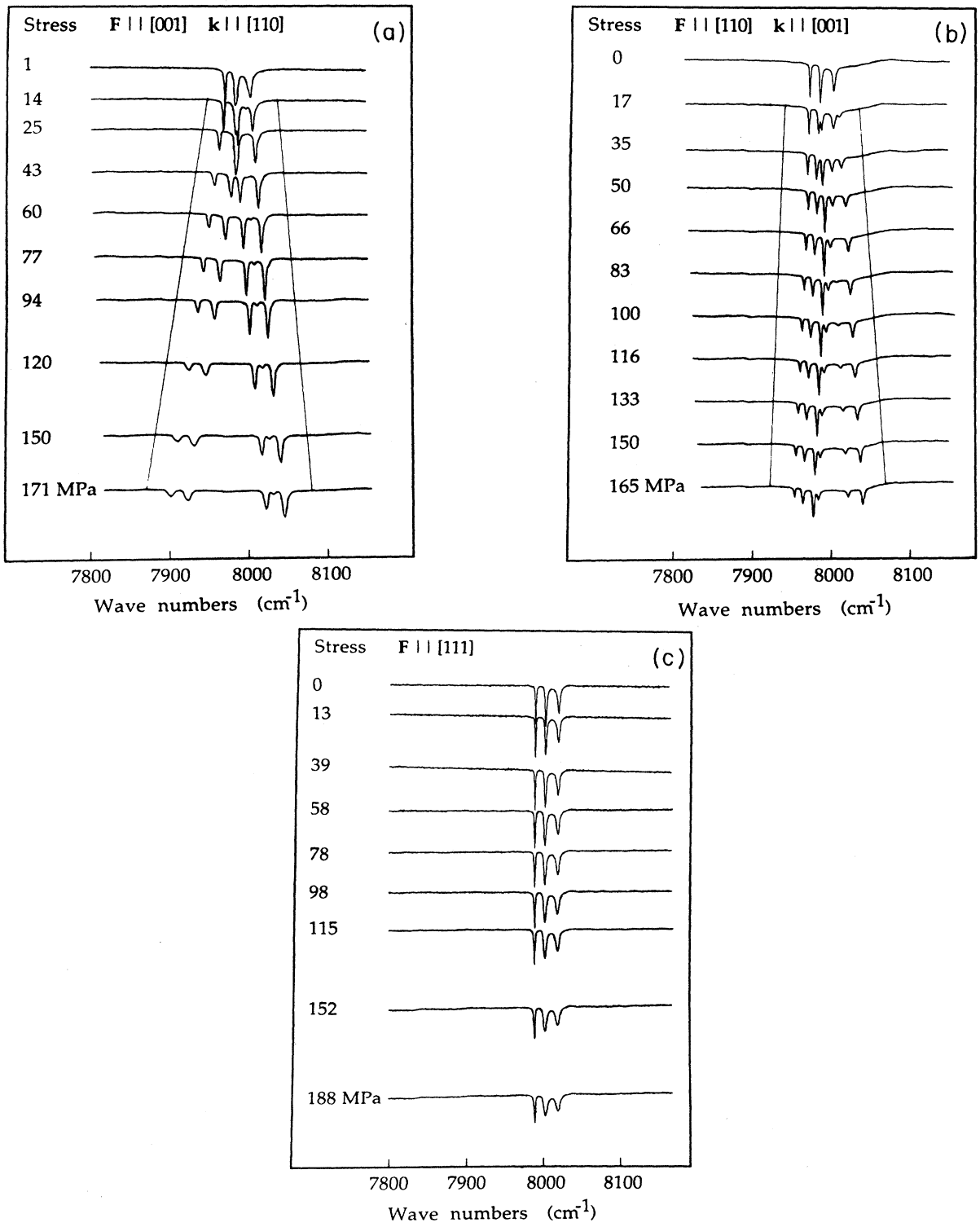

FIG. 2. Transmission spectra showing the response of the T lines to uniaxial stress parallel to (a) [001], (b) [110], and (c) [111]. The straight lines indicate the stress shifts of the unequivalent conduction-band minima.

that no splitting and only a small center-of-gravity shift is observed for stress parallel to [111], whereas large splittings are observed for both the [001] and [110] directions. The nonsplitting behavior for [111], and the stress-induced linear shift rates at higher stresses for the [001] and [110] directions are characteristic of the conduction-band minima in silicon. In order to make this observation more transparent, the straight lines in Fig. 2 represent the stress response of the conduction-band minima of silicon. The close agreement immediately suggests that the T-line final states are associated with the conduction-band minima. It may therefore be assumed that at least the final states of the transitions involve donor states which can be described by EMT and DPA. It may further be concluded that the T lines have a common origin since the stress components show avoided crossing behavior due to mixing effects at about 25 MPa for stress parallel to [001] and at about 50 MPa for stress parallel to [110]. Such behavior is only possible for states belonging to the same center. The nonsplitting behavior seen for stress along [111] and the close agreement between the experimental data and DPA for the other two stress directions, suggests that no orientational degeneracy is present at the T-line center. It is very important to emphasize that there may be other effects that make an orientational degeneracy difficult to detect. One such effect is stress-induced reorientation, previously reported for the Pt^- center.[15] However, it is possible to analyze our data, assuming tetrahedral symmetry and, we comment further below on the possibility of a symmetry lower than T_d for this defect.

At higher stress parallel to [110], the T lines split into six components. In the case of [001] stress, five components are readily observed. However, a close inspection reveals six lines for [001] stress and the sixth line, although of low intensity, is found on the high-energy side of the upper component of the T_3 line at higher stress. The number of stress-induced components observed for stress parallel to [001] and [110] is six, which equals the number of conduction-band minima in silicon. This gives an important piece of information in the theoretical evaluation of the experimental data.

The theoretical model, presented below, is thus based on EMT and DPA. It is well known that deep levels in silicon may have a series of excited states bound by the screened Coulomb potential. In the case of shallow donors, the excitation spectra show transitions only to shallow p-like states, which under uniaxial stress follow their respective band edges rigidly. Deep-level excitation spectra show, however, in most cases, in addition to the p-lines, excitations to s-like states. Assuming that the T lines involve p-like donor states, it is most probable that not only a few but a complete series in a narrow-energy range should be observed, as in the case of shallow group-V and the deep chalcogen donors. We therefore assume that the T-line spectrum involves transition to s-like donor states, as in the case of the Ag-related donor in Si.[12] It is interesting to note that an s state is sixfold degenerate (excluding spin) due to the six equivalent conduction-band minima of silicon, a degeneracy which equals the number of stress-induced components observed for the T lines. This sixfold degeneracy is, for all donors in silicon, known to be at least partly lifted by the valley-orbit interaction and central-cell effects, in accordance to the relevant point-group symmetry.

IV. THEORETICAL CONSIDERATIONS

A. Model for the center

We consider the final states as being built up from an originally sixfold degenerate shallow-donorlike s state. It is well known that for tetrahedral centers, e.g., the shallow group-V donors and the deep chalcogen donors, the s states are split into an orbital singlet $ns(A_1)$, a doublet $ns(E)$, and a triplet $ns(T_2)$. In the case of, for example, the chalcogen donors, the ground state was experimentally shown to be $1s(A_1)$, in accordance with full theoretical calculations.[16] However, we assume, for reasons to be discussed below, that the central-cell potential of the T line center is not able to substantially alter the binding energy of any of the EMT-like donor states. For a given s-like donor state, therefore, all the six linear combinations are nearly degenerate and we consider the A_1, E, and T_2 combinations of an s-like state as final states in the T-line transitions.

The orbital parts of the wave functions are written as symmetry-adapted linear combinations of the six conduction-band minima:

$$\Psi=\sum_{j=1}^{6}\alpha_j F_j(\mathbf{r})\phi_j(\mathbf{r}) , \tag{1}$$

where $F_j(\mathbf{r})$ are the EMT-envelope functions and $\phi_j(\mathbf{r})$ is the Bloch function for the jth minimum. The coefficients α_j are determined from symmetry considerations and are given by

$$\begin{array}{lll} A_1 & a_1 & (1/\sqrt{6})(1,1,1,1,1,1); \\ E & \theta & (1/\sqrt{12})(-1,-1,-1,-1,2,2), \\ & \varepsilon & (1/2)(1,1,-1,-1,0,0); \\ T_2 & x & (1/\sqrt{2})(1,-1,0,0,0,0), \\ & y & (1/\sqrt{2})(0,0,1,-1,0,0), \\ & z & (1/\sqrt{2})(0,0,0,0,1,-1); \end{array} \tag{2}$$

where the vectors indicate the contributions from the $\mathbf{x}$, $-\mathbf{x}$, $\mathbf{y}$, $-\mathbf{y}$, $\mathbf{z}$, and $-\mathbf{z}$ conduction-band valleys, respectively. The excited electron has a spin of $\frac{1}{2}$. The spin-$\frac{1}{2}$ functions span the Γ_6 irreducible representation of the $\bar{T}_d$ double group. Taking spin into account, the irreducible representation for the combined states are given by the direct product between Γ_6 and the orbital parts (A_1, E, and T_2). $A_1\times\Gamma_6$ transforms as Γ_6, $E\times\Gamma_6$, as Γ_8, and $T_2\times\Gamma_6$ as $\Gamma_7+\Gamma_8$. The spin-orbit interaction is important for the electronic structure of the heavier group-V donors and the EMT-like donor states of the chalcogen double donors. Considering the heavy element Pt, this may very well be the case for the T-line center and in our model we invoke a splitting of the T_2 state

into a Γ_7 and a Γ_8 state due to the spin-orbit interaction. The spin-orbit term in the Hamiltonian transforms according to the totally symmetric A_1 irreducible representation and, hence, it may also mix states of equal symmetry, e.g., the Γ_8 states derived from E and T_2.

B. Spin-orbit interaction

The spin-orbit Hamiltonian in T_d symmetry is given by

$$H_{\text{s.o.}}=\frac{h}{4m^2c^2}(\nabla U\times\mathbf{p})\cdot\boldsymbol{\sigma}=\mathbf{V}\cdot\boldsymbol{\sigma}\ . \tag{3}$$

We define two spin-orbit parameters, ξ_1 and ξ_2, which describe the spin-orbit interaction within the manifold of T_2 states giving rise to the splitting between $\Gamma_7(T_2)$ and $\Gamma_8(T_2)$ and the coupling between the $\Gamma_8(T_2)$ and $\Gamma_8(E)$ states, respectively. ξ_1 and ξ_2 are defined by

$$\begin{aligned}\xi_1&=-2i\langle T_2,x|V_y|T_2,z\rangle\ ,\\ \xi_2&=i\sqrt{\tfrac{3}{2}}\langle E,\varepsilon|V_z|T_2,z\rangle\end{aligned} \tag{4}$$

in accordance with Ref. 17. The spin-orbit matrix is presented in the Appendix.

C. Uniaxial stress

The shift of the jth conduction-band minimum under uniaxial stress was calculated using DPA. The jth conduction-band minimum has stress-induced energy shift, with respect to the center of gravity of the conduction bands, given by

$$\delta E^{(j)}=\Xi_u(s_{11}-s_{12})[(\mathbf{n}\cdot\mathbf{j})^2-\tfrac{1}{3}]T\ , \tag{5}$$

where Ξ_u is the shear deformation potential, s_{11} and s_{12} are components of the elastic compliance tensor, $\mathbf{n}$ is a unit vector along the applied uniaxial stress, $\mathbf{j}$ is a unit vector along the direction of the jth minimum, and T is the magnitude of the applied stress. T is defined to be negative for compressional stress. The matrix elements of the stress operator V between the 12 basis functions is easily obtained by first noting that V is diagonal in spin and then applying V between the functions given by Eq. (2) and using the energy shifts in Eq. (5). The matrix elements of the stress operator are given by

$$\langle\psi_m|V|\psi_n\rangle=\sum_{j=1}^{6}\alpha_j^{(m)}\alpha_j^{(n)}\delta E^{(j)} \tag{6}$$

and are presented in the Appendix in terms of $\Delta=\Xi_u(s_{11}-s_{12})T/3$. The stress response of the T_2 states is diagonal whereas the A_1 and E_θ states may mix, as has previously been experimentally observed for shallow donors[18] in Si. An inspection of the stress matrix shows that the manifold of EMT-like donor states is not sensitive to stress parallel to the [111] direction since all $\langle 100\rangle$ valleys have the same angle to the [111] direction.

D. Zeeman splitting

The Zeeman Hamiltonian for a single electron in a magnetic field $\mathbf{B}$, is given by

$$H_z=\mu_B(g_1\mathbf{l}+g_s\mathbf{s})\cdot\mathbf{B}\ , \tag{7}$$

where μ_B is the Bohr magneton, g_1 is the orbital g factor, and g_s is the spin g factor. The basis functions are chosen as $|\Gamma\mu\rangle|m_s\rangle$, where Γ is an irreducible representation of the orbital part (A_1, E, or T_2) and μ is the row index. ($|m_s\rangle$ are the usual basis functions α and β for $s=\frac{1}{2}$.) The angular momentum operators $\mathbf{l}$ and $\mathbf{s}$ transform according to the irreducible representation T_1 in T_d symmetry and a matrix element between the chosen basis functions, $|\Gamma\mu\rangle|m_s\rangle$, may be simplified to read

$$\begin{aligned}\langle\Psi'|H_z|\Psi\rangle=\mu_B\mathbf{B}(&g_1\langle\Gamma\mu'|\mathbf{l}|\Gamma\mu\rangle\langle m_s'|m_s\rangle\\&+g_s\langle m_s'|\mathbf{s}|m_s\rangle\langle\Gamma'\mu'|\Gamma\mu\rangle).\end{aligned} \tag{8}$$

The first term is diagonal in spin whereas the second is diagonal in the orbital part.

Firstly, the first term in Eq. (8) is to be discussed. The matrix elements involving the A_1 state are zero, since the direct product $A_1\times T_1$ does not contain A_1, E, or T_2. Since $\mathbf{l}$ is an off-diagonal operator within the T_2 manifold (row index$=x$, y, and z), the only possible nonvanishing matrix elements are between different valley pairs. These intervalley matrix elements have, however, been shown to be zero for EMT donor states.[19,20] The matrix elements with the E manifold are certainly zero, since $E\times T_1$ does not contain E. Group-theoretical considerations alone cannot exclude off-diagonal terms between the E and the T_2 states since the direct product $E\times T_1=T_1+T_2$ contains T_2. Using the Wigner-Eckart theorem matrix elements of the type

$$\langle E\mu|\mathbf{l}\mu'|T_2\mu''\rangle=\langle E\mu|T_1T_2\mu'\mu''\rangle[E|T_1|T_2] \tag{9}$$

are obtained, where the coupling coefficients $\langle E\mu|T_1T_2\mu'\mu''\rangle$ can be found in, e.g., Griffith's tables.[21] $[E|T_1|T_2]$ is the reduced matrix element, independent of μ, μ', and μ''. The coupling coefficient of e.g. the matrix element $\langle E\varepsilon|\mathbf{l}z|T_2z\rangle$ is found to be nonzero. However, an inspection of Eq. (2) shows that this matrix element couples differently valley pairs and, therefore, it must equal zero. Accordingly, we conclude that the operator $\mathbf{l}$ has vanishing matrix elements in the manifold of A_1, E, and T_2 EMT-like states and that $g_1=0$ as long as the states are well accounted for by EMT, as suggested by their stress response.

The second term in the Zeeman Hamiltonian may be calculated from, for example, Griffith's coupling coefficient tables. This term is diagonal in the orbital part of the wave functions and the Zeeman matrix (excluding spin-orbit elements) becomes very simple, having a block-diagonal structure of 2×2 matrices. In our calculations we use $g_s=2$. The Zeeman matrix is presented in the Appendix.

E. Intensity calculations

When calculating the relative intensities and polarization rules, the symmetry of the ground state must be known. As discussed below, a Γ_7 ground state constructed from a spin-orbit split T_2 state is assumed. The

electric-dipole operator **D** transforms as T_2 in T_d symmetry. The direct product $\Gamma_7 \times T_2 = \Gamma_6 + \Gamma_8$ shows that transitions to a Γ_7 state are forbidden, whereas transitions to states of Γ_6 and Γ_8 symmetry are allowed. The eigenstates of the stress and Zeeman matrices are linear combinations of our basis functions, $|\Gamma\mu\rangle\,|m_s\rangle$. **D** cannot flip spin and its matrix elements are therefore determined by the orbital parts of the wave functions. The electric-dipole matrix elements are therefore generally a sum over matrix elements of the type $T_2 \rightarrow A_1$, $T_2 \rightarrow E$, and $T_2 \rightarrow T_2$, where the T_2 state on the left-hand side and the irreducible representations on the right-hand side indicate the orbital part of the ground and the final state, respectively. In our fitting procedure of the intensity, we make use of the three parameters, α_1, α_2, and α_3, proportional to the reduced matrix elements for the $T_2 \rightarrow A_1$, $T_2 \rightarrow E$, and $T_2 \rightarrow T_2$ transitions, respectively. The values of α_1, α_2, and α_3 were found by obtaining the best agreement for both the Zeeman and the stress data.

V. RESULTS AND DISCUSSION

A. Uniaxial stress

In Fig. 3, the splittings of the T lines for uniaxial stress applied parallel to the [001], [110], and [111] directions are presented. The eigenvalues of the full-stress matrix have been fitted to the experimental data to obtain the best agreement for the stress and Zeeman spectra simultaneously. The values of the spin-orbit parameters ξ_1 and ξ_2 that gave the best fit are -3.7 and $|5.2|$ cm^{-1}, respectively and the energies of the donor states in absence of the spin-orbit interaction were determined to be $E(A_1)=7981.0$ cm^{-1}, $E(E)=7995.3$ cm^{-1}, and $E(T_2)=8010.0$ cm^{-1}. The value used for Δ was 0.227 cm^{-1}/MPa. In Fig. 3, the lines at zero stress have been relabeled in accordance with our model as follows: $T_1 \rightarrow \Gamma_6(A_1)$, $T_2 \rightarrow \Gamma_8(E)$, and $T_3 \rightarrow \Gamma_8(T_2)$. In addition there is a $\Gamma_7(T_2)$ component, which is invisible at zero stress. This new labeling scheme will be used throughout this paper. When stress is applied, the symmetry is lowered from $\bar{T}_d$ to $\bar{D}_{2d}$ and $\bar{C}_{2v}$ for stress parallel to [001] and [110], respectively. The stress-split components have been labeled $X_6(n)$, $X_7(n)$, and $\Lambda_5(n)$, these being irreducible representations of the $\bar{D}_{2d}$ and the $\bar{C}_{2v}$ double groups, respectively, and n indicates the level ordering in the figure. It must be emphasized that the states $\Gamma_8(E)$ and $\Gamma_8(T_2)$ include both E and T_2 character since they are mixed by the spin-orbit interaction, however, our labeling scheme indicates the dominant contribution.

The line at lowest energy $\Gamma_6(A_1)$ is sensitive only to the hydrostatic component of the stress unless mixed with other states of equal symmetry. This can be readily observed at very low stresses parallel to [001] in Fig. 3(a), where the admixture with one of the $\Gamma_8(E)$ components is still negligible. The two states of equal symmetry, $X_6(1)$ and $X_6(2)$, show an avoided-crossing behavior below 30 MPa. At higher stresses, $X_6(1)$ contains contributions only from the z valleys, whereas, $X_6(2)$ only contains contributions from the x and y valleys, as mirrored by their stress response. The small hydrostatic stress

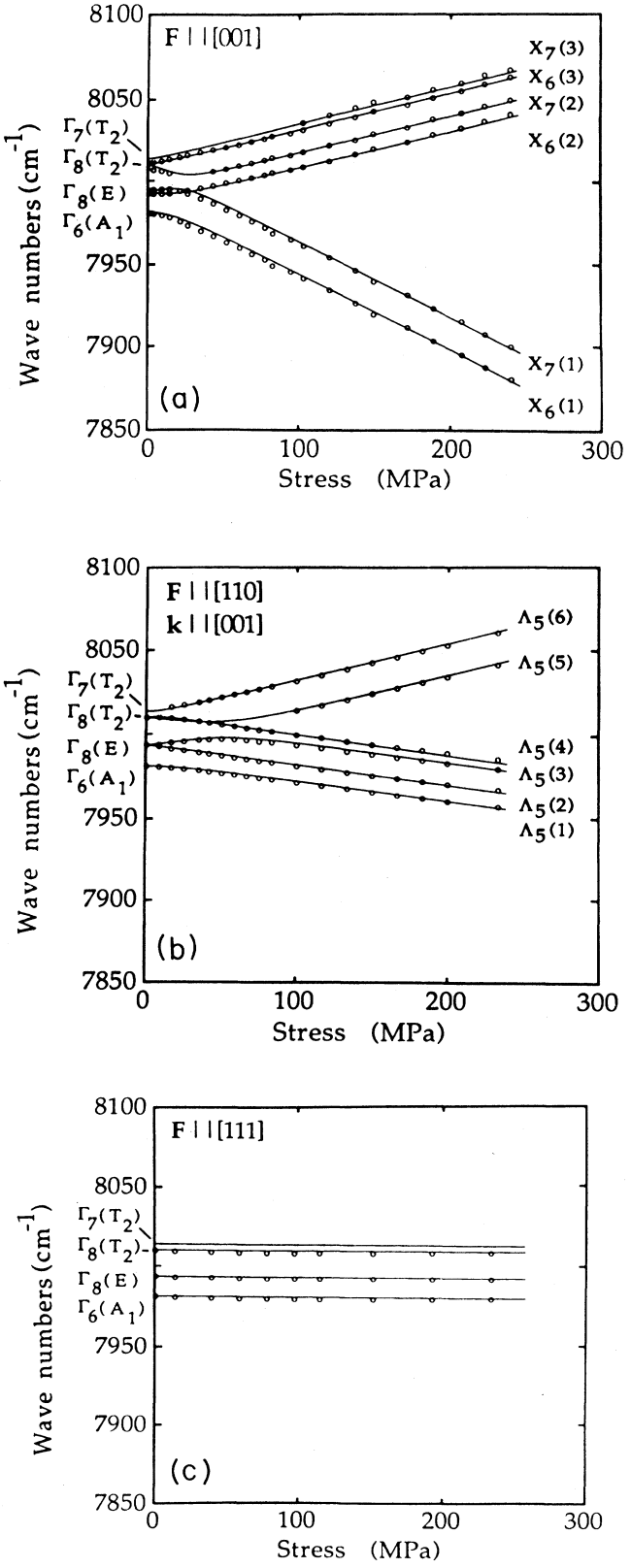

FIG. 3. The stress response of the T lines for stress applied parallel to (a) [001], (b) [110], and (c) [111]. The open circles are the experimental data and the solid lines are obtained from the theoretical model. For the labeling of the components, see text.

response of $\Gamma_6(A_1)$ is observed more transparently for [110] stress [Fig. 3(b)], since higher [110] stress is needed to bring the A_1 component close to the E_θ component.

The line at 7994 cm^{-1}, labeled $\Gamma_8(E)$ in T_d symmetry, splits into two components, $X_6(2)$ and $X_7(1)$. The $X_6(2)$ state moves towards lower energies approximately as $-\Delta$ for low stresses while the admixture with the $X_6(1)$ state is still negligible. Due to the repulsion of $X_6(1)$, the stress shift for $X_6(2)$ changes to Δ and $X_6(2)$ moves towards higher energies. The admixture between $X_6(1)$ and $X_6(2)$ is due to a stress induced mixing of the A_1 and E_θ orbitals which leads to a decoupling of the z and the x,y valley pairs at higher stress. The other $\Gamma_8(E)$ component, $X_7(1)$, shifts for smaller stresses approximately as Δ approaches the $X_7(2)$ component and is then repelled due to the spin-orbit interaction. The two lines into which the $\Gamma_8(E)$ is split at very low stress will therefore approach each other and cross at about 25 MPa without showing any avoided-crossing behavior since they belong to different irreducible representations. This crossing is very accurately reproduced by our theoretical model, the energies of which are obtained from the eigenvalues to the stress matrix in the appendix. At higher stress, the energy of the stress splittings exceeds both the valley-orbit and spin-orbit energies which leads to a linear-stress response with shift rates equal to those of the six conduction-band minima. The $\Gamma_7(T_2)$ line is invisible at zero stress but becomes weakly visible at higher stresses as a high-energy partner to $X_6(3)$. This makes the determination of its energy position less reliable.

In Fig. 3(b) the splitting for stress in parallel to [110] for the wave vector of the photons, **k**, parallel to [001] is presented. The same splitting behavior is observed for $\mathbf{k}\|[\bar{1}10]$ although the lines are observed with different relative intensities. All six stress-induced components could be clearly followed as a function of stress. It is interesting to note that the $\Gamma_7(T_2)$ line, only weakly visible for [001] stress, becomes one of the strongest lines at higher stresses, as is readily seen by a comparison between Figs. 2(b) and 3(b). In this case the theoretical model is also able to predict the splitting behavior with high accuracy by using the same parameters as in the case of [001] stress.

Figure 3(c) shows the response of all three lines for stress in the [111] direction. The six conduction-band minima have the same angle to the [111] axis and all six valleys experience the same energy shift. No splitting is therefore expected, as experimentally observed. The only effect is the hydrostatic shift which was determined from this measurement and found to be small, only 0.011 cm^{-1}/MPa. This hydrostatic shift rate has been included in the [001] and [110] fits.

The stress data are very well fitted by the T_d-donor model. One may expect to have detected a symmetry lower than T_d for this Pt-related center, since the single substitutional center, Pt^-, has a C_{2v} symmetry and complex centers by necessity have a lower symmetry than T_d. It is reasonable to assume that even in the case when the delocalized excited states are not perturbed by a central-cell potential lower than T_d symmetry, the ground state should be strongly affected which should show up as an orientational degeneracy. No such degeneracy was observed and for all stress directions, a common hydrostatic shift was found.

The experimental data and a comparison with the electronic structure of the heavier group-V and substitutional chalcogen donors in Si may suggest another model for the T-line center. This alternative model has to be discussed, since it is a natural extension of the electronic properties of these well-known centers which have the $1s(A_1)$ state as ground state. The A_1 symmetry allows electric-dipole transitions to the valley-orbit split $1s(T_2)$ state only which, although EMT forbidden, becomes visible for those centers where the ground state deviates considerably from EMT. The $1s(T_2)$ donor state is split into a Γ_7 and a Γ_8 state by the spin-orbit interaction. This may account for two of the T lines visible at zero stress, and in order to obtain three lines, a D_{2d} distortion, or one of its subgroups, has to be assumed, lifting the degeneracy of the Γ_8 state. As a result, three lines (Kramer doublets) should be observed at zero stress. The T_2-orbital states are thus quantized along the D_{2d} axis of the center of the observed splitting, e.g., for [001] stress, is due to the different stress response for centers having their axis parallel or perpendicular to the [001] stress direction. This model gives rise to six components for [001] and [110] stress and accounts rather well for the overall splittings at higher stress, but does not predict the correct stress behavior at lower stress. In addition, this model predicts two stress-induced lines originating from the $\Gamma_6(A_1)$ line, which are not experimentally observed and, furthermore, this model is not able to predict the weak $\Gamma_7(T_2)$ line for the [001] stress.

B. Zeeman results

The Zeeman splittings of the T lines were observed to be identical for magnetic fields parallel to [001], [110], and [111]. The Zeeman pattern is shown in Fig. 4 for $\mathbf{B}\|[001]$. For this direction of the magnetic field, the Zeeman Hamiltonian is diagonal when neglecting the

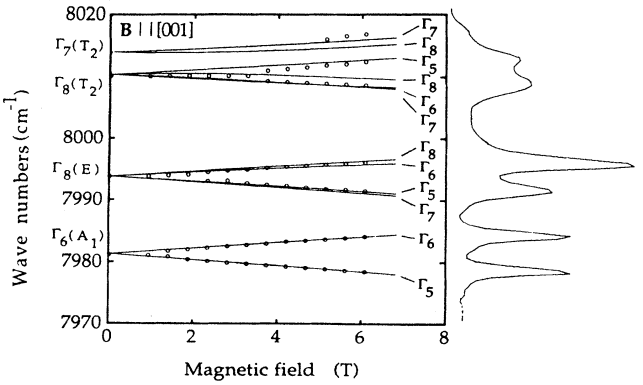

FIG. 4. The Zeeman splittings of the T-line center for $\mathbf{B}\|[001]$. The open circles are the experimental data and the solid lines are obtained from the theoretical model using $g_l=0$ and $g_s=2$ and the same fitting parameters as for the stress model. In addition, the spectrum for $B=6$ T is present.

spin-orbit matrix elements (see appendix). The splitting of the $\Gamma_6(A_1)$ line is therefore linear, since the magnetic field does not affect the valley-orbit splitting. The experiment offers an excellent check of our model, interpreting the T lines as transitions to EMT s states. For such states $g_l=0$, as discussed above, and only the spin has to be considered. By using $g_s=2$ and the wave functions used previously, a fit to the Zeeman data was obtained which is presented in Fig. 4, together with the experimental results. Since the splittings are relatively small, the line positions are less certain for low magnetic fields, and especially for the lines in the $\Gamma_8(T_2)$ manifold. In this case, only the central peak value has been plotted in Fig. 4 for magnetic fields up to about 4 T.

The four $\Gamma_8(E)$ states would have shown identical splitting to that observed for the $\Gamma_6(A_1)$ states unless they were mixed with T_2 states by the spin-orbit interaction. The small additional splittings of the $\Gamma_8(E)$ main components, as implied by our model, were too small to be experimentally resolved. The energy positions of $\Gamma_8(T_2)$ components are difficult to measure below about 4 T, whereas a satisfactory agreement between experimental data and theory was achieved for higher fields. At higher fields, the $\Gamma_7(T_2)$ lines gain in intensity by mixing with some of the $\Gamma_8(T_2)$ compounds but their energy positions have been determined with some ambiguity since they are not clearly resolved.

The good agreement between experimental stress and Zeeman data and the T_d model proposed strongly suggests that the electron in the excited state is found in one of the six valley-orbit-split s-like donor states. The fitting procedure so far only considered the excited-electron states whereas in the intensity calculations, knowledge of the initial state in the transitions is necessary. The electric-dipole operator D does not flip the electron spin and accordingly, its matrix elements are diagonal in spin. In T_d symmetry $\mathbf{D}$ transforms as the T_2 irreducible representation. The orbital part of the ground-state wave function of the T-line center must allow transitions to states of A_1, E, and T_2 symmetry which is possible only if the ground state has a T_2 orbital part. The correct ground state to be chosen is determined by the observation that the $\Gamma_7(T_2)$ line was invisible in the limit of zero perturbations. Symmetry considerations show that transitions from a Γ_7 ground state are allowed to all excited states *except* to $\Gamma_7(T_2)$. We therefore assume a Γ_7 ground state, a choice which gives the correct intensity and polarization rules (see below). This state is obtained if the spin-orbit coupling splits the T_2 ground state into a fourfold degenerate Γ_8 state and a twofold degenerate Γ_7 state.

C. Relative intensities and polarization rules

In order to further test our assignment of the ground and excited states, the relative intensities as well as the polarization rules of the stress and Zeeman-split components were calculated. In Fig. 5 the experimentally found relative intensities from our stress measurements are compared with those given by our theoretical model using $\alpha_1=-0.410$, $\alpha_2=-0.205$, and $\alpha_3=0.405$. Although the relative intensities are not perfectly reproduced, the overall behavior is found to be well reproduced by our model. It should be pointed out that in some cases it was impossible to measure the relative intensity at lower stress due to overlap of various lines. In Fig. 6 the results of the polarization experiments are compared with the values obtained from theory. The polarized intensities were measured with the electric field of the photons parallel ($\mathbf{E}\|\mathbf{F}$) or perpendicular ($\mathbf{E}\perp\mathbf{F}$) to the stress axis. Our model is able to accurately reproduce the main features obtained in the polarization experiment.

The relative intensities and polarization rules were also calculated for the Zeeman experiment. The results for $\mathbf{B}\|[001]$ and $B=6$ T are presented in Fig. 7 and it is readily seen that the observed intensities are well reproduced by our calculation. It must be pointed out that in order to reproduce the experimentally observed intensities we have to include contributions to the intensity from *both* $m_j=\pm\frac{1}{2}\Gamma_7$ ground states and, thus, the good agreement between experiment and model shows that a splitting of the Γ_7 ground state is too small to be detected by our experiment.

D. Doping and annealing experiments

The intensity ratio between the T and the Pt-acceptor lines is strongly dependent on the Fermi-level position in the starting material but they were both observed simultaneously in all our Pt-doped samples. It was found that the intensity of the T lines increases with increasing shallow-acceptor concentration, whereas the intensity of the acceptor lines decreases. This shows that the T lines and the acceptor transitions have different ground states. It has been suggested that the single substitutional Pt impurity in silicon is an amphoteric center, i.e., it may be found in the single negative and positive charge states, as well as in its neutral charge state. A similar behavior is also expected for the single substitutional gold impurity in silicon. In the case of gold, both line spectra as well as deep-level transient spectroscopy signals have been attributed to the donor and acceptor levels. Although the T-line spectrum involves transitions to shallow-donor states, the spectrum is not a candidate for the $0/+$ donor transitions of the substitutional Pt center since both the T lines and the acceptor transitions should then have the same initial state and, hence, should show the same trend in the doping experiments. Furthermore, the transition energies of the T lines are not consistent with the binding energy obtained earlier for the Pt donor.[3]

An isochronal annealing experiment was performed on a p-type (boron-doped) sample of initially 14 Ω cm resistivity in which both the T lines and the acceptor lines were observed in transmission with relatively high intensity. In this sample, Pt^- was observed in EPR only under illumination. The annealing time was 30 min and the change in relative intensity between the T lines, the acceptor lines, and the Pt^- EPR center was monitored after

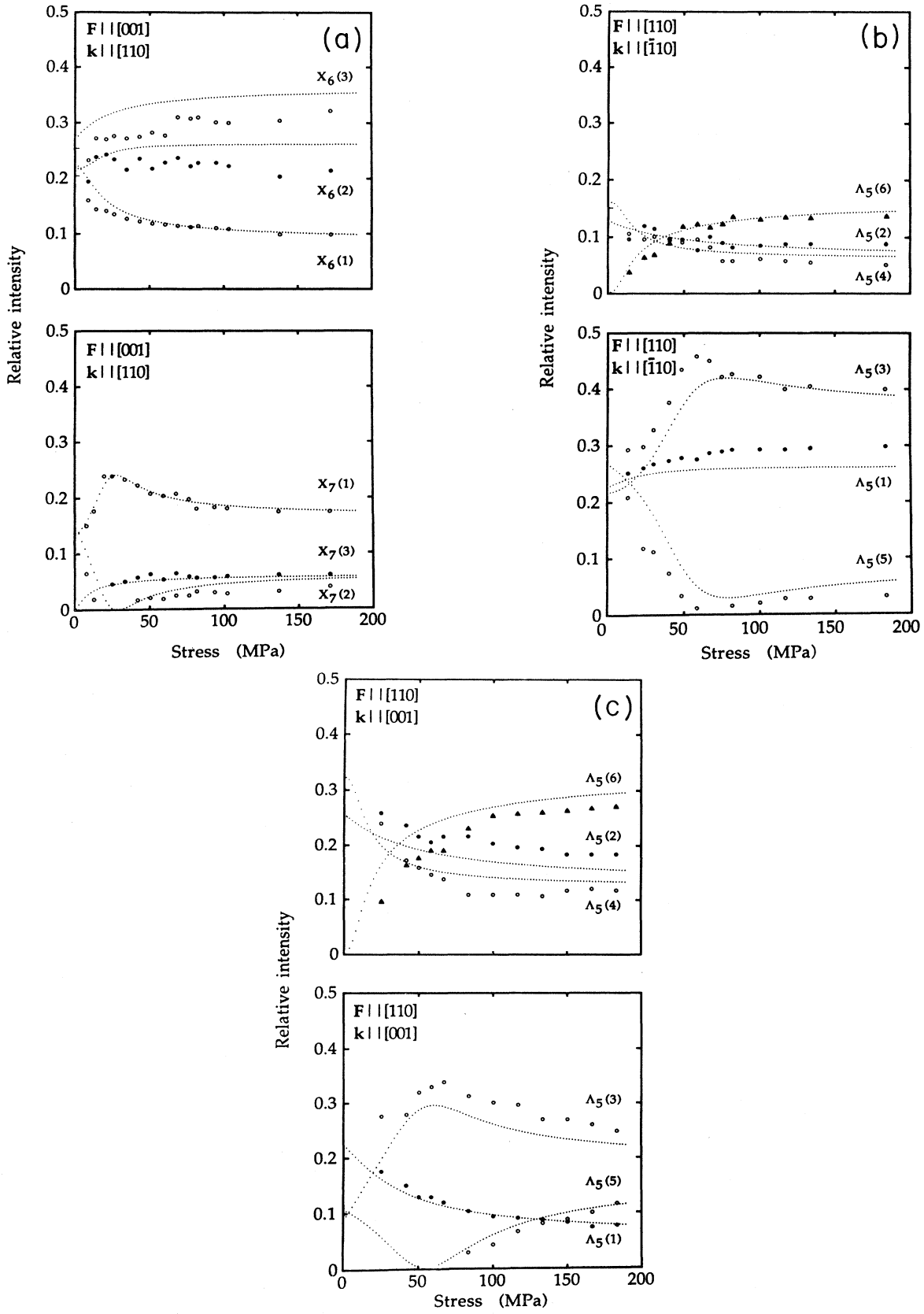

FIG. 5. The intensity of the T lines as a function of stress. (a) $\mathbf{F}\|[001]$ and $\mathbf{k}\|[110]$, (b) $\mathbf{F}\|[110]$ and $\mathbf{k}\|[\bar{1}10]$, and (c) $\mathbf{F}\|[110]$ and $\mathbf{k}\|[001]$. The labeling of the lines is in accordance with that in Fig. 3.

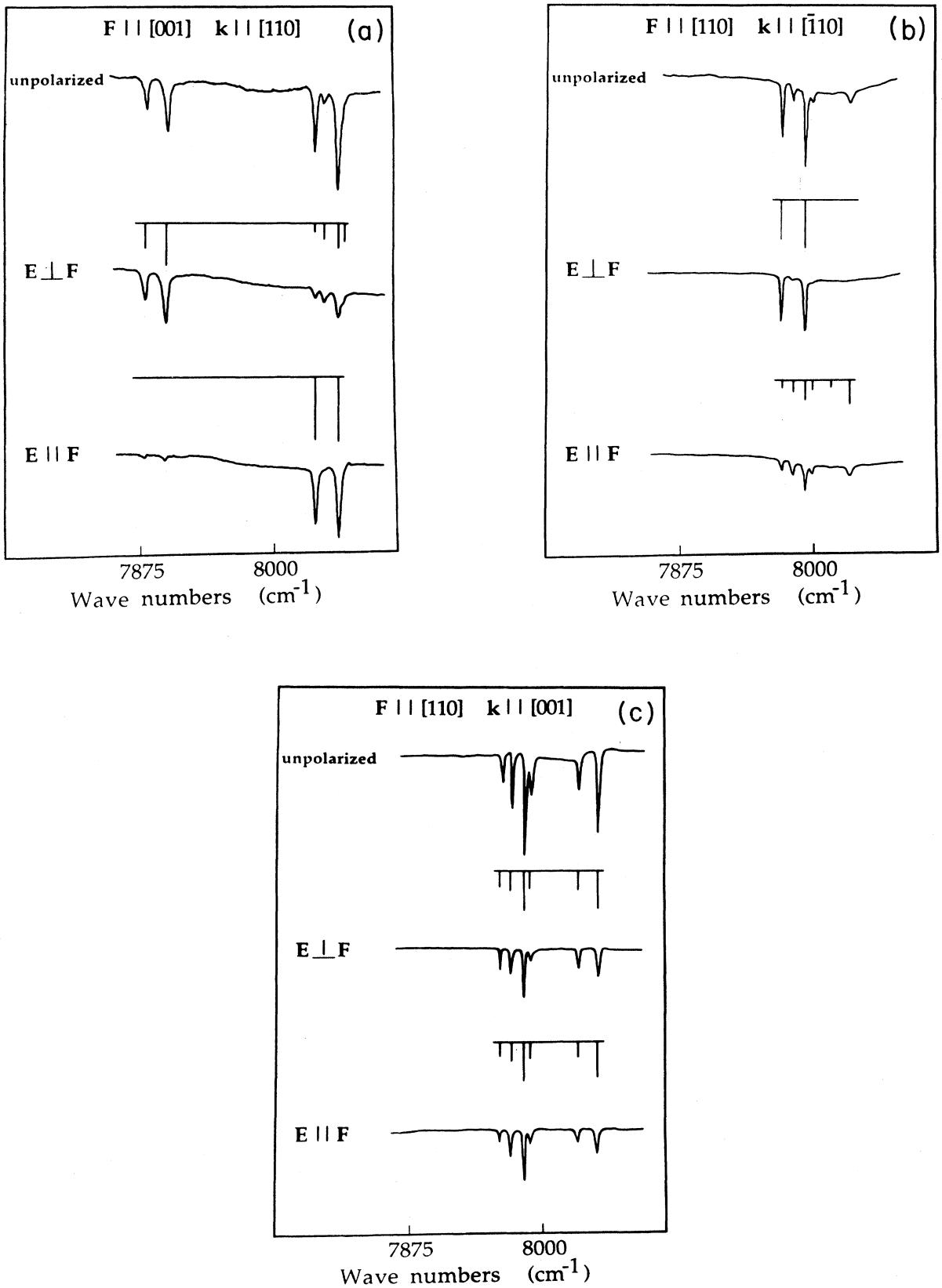

FIG. 6. The experimentally measured polarized, relative intensities of the stress-split components of the T lines, compared with those given by the donor model. (a) $\mathbf{F}\|[001]$, $\mathbf{k}\|[110]$, and $T=240$ MPa, (b) $\mathbf{F}\|[110]$, $\mathbf{k}\|[\bar{1}10]$, and $T=125$ MPa, and (c) $\mathbf{F}\|[110]$, $\mathbf{k}\|[001]$, and $T=200$ MPa.

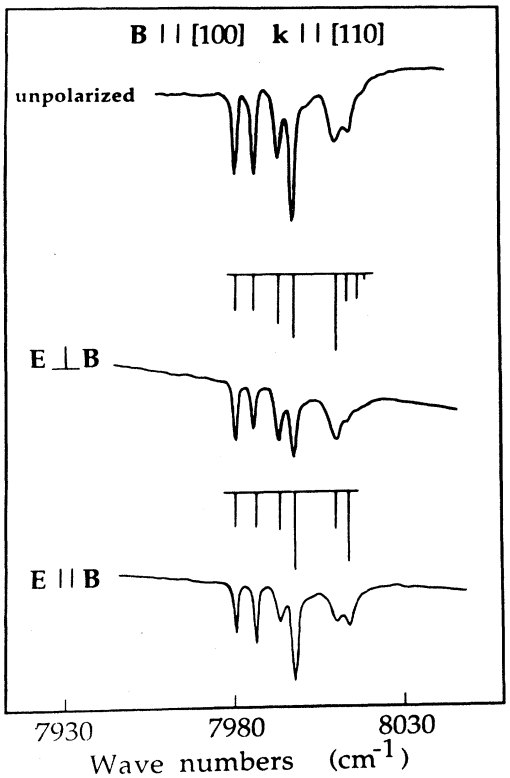

FIG. 7. The polarized relative intensities, obtained in the Zeeman experiment for $\mathbf{B}\|[001]$ and $\mathbf{k}\|[110]$ in comparison with the calculated values. The magnitude of the magnetic field is 6 T.

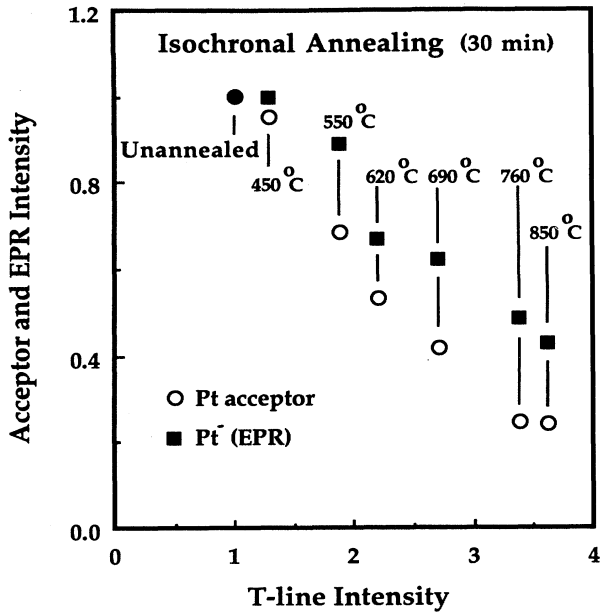

FIG. 8. The intensity of the Pt acceptor (absorption) and Pt^- (EPR) as a function of the intensity of the T lines (absorption) obtained from the annealing experiment on the same sample. The resistivity prior to the Pt doping was 0.6 Ω cm p type. The intensities of the unannealed samples are normalized to 1.

each annealing step. It was found that the intensity of the acceptor lines and Pt^- decreased while the intensity of the T lines increased (see Fig. 8). This may indicate that as substitutional Pt centers disappear, new T-line centers are formed. This assumption is, however, ruled out by an additional experiment. In samples of originally low resistivity (0.6 Ω cm) p type (very low transmission signal from the acceptor) the intensity of the T lines as well as the Pt^- EPR signal did not change in a similar annealing experiment to the one described previously. These experiments strongly suggest that the change in relative intensities in the 14 Ω cm p-type sample is not due to production of T-line centers at the expense of substitutional Pt centers, but rather an effect due to a change in the Fermi-level position in the material.

The annealing and EPR experiments could unfortunately not give any information which could be used to unambiguously identify the chemical origin of the T-line center. However, it is possible to tentatively assign its origin based on the wealth of information gained from the various experiments carried out, and which can be shortly summarized: the center is well described by a model of tetrahedral symmetry, p-type material favors the T-line center and decreases the concentration of neutral substitutional Pt centers, the T lines are due to excitations to shallow donorlike states, and, finally, the T lines are not due to the donor transition $Pt^0 \rightarrow Pt^+ + e^-$. These results indicate that the T lines are due to the double-donor transition $Pt^+ \rightarrow Pt^{2+} + e^+$ at the single substitutional Pt center.

VI. MICROSCOPIC MODEL

It is not possible to define a microscopic model for the T-line center unambiguously and this section should be considered as a discussion of a plausible model in the light of the known properties of Pt^-. It was not necessary to invoke reorientation effects in our model and we conclude that the actual symmetry of the center is T_d. Theoretical calculations on the substitutional platinum center in silicon show that the bound state in the band gap is a vacancylike t_2 state. These results are in agreement with the Watkins vacancy model in which the Pt atom with a $5d^{10}$ closed-shell configuration enters a vacancy. The electronic properties are mainly given by the vacancy. Pt has an atomic configuration of $5d^9 6s^1$ and it is assumed that the $6s$ electron enters the d shell. The different charge states of Pt should then resemble the corresponding charge states of the vacancy. This model has been successfully applied to the electronic properties of Pt^- observed in EPR. The t_2-gap orbital of platinum is sensitive to Jahn-Teller (JT) distortions similar to those occurring for the silicon vacancy. Whereas the spin-orbit could be excluded for the vacancy it may be of great importance in the case of Pt. The spin-orbit interaction and the JT effect are competing processes. On the one hand, the JT effect gives rise to a quenching of, e.g., the orbital g factor and the spin-orbit interaction (Ham effect) and, on the other hand, the spin-orbit interaction may stabi-

lize the center against JT distortions.

In the microscopic model for the T-line center we assume, in accordance with the one-electron model for V^+, that the T_2-gap state is occupied by a single electron. The spin-orbit interaction splits the T_2 state into a Γ_7 and a Γ_8 state. Only the Γ_8 state is JT active and in the case when the lowest state is Γ_7, the JT effect acts only in second order due to mixing with the Γ_8 state. The observed T_d symmetry leads to the assumption that the spin-orbit interaction is stronger than the JT effect and stabilizes the center against distortions. A cluster calculation[22] on the electronic structure of Pt including the spin-orbit interaction, did not show a large spin-orbit splitting of the T_2 state of platinum. However, our wealth of experimental data strongly suggests such a spin-orbit splitting. It is difficult to exclude a small admixture between the Γ_8 and Γ_7 states due to second order JT effects in the dynamical regime since it should not affect the splitting behavior (assuming no preferential stress alignment) but only the intensity and the polarization rules which are difficult to obtain with high accuracy.

In the case of the chalcogen deep donors it may be pertinent to discuss a central-cell correction although the ground state contains contributions not only from the conduction-band minima. The $1s(A_1)$ state is the only linear combination that has a nonvanishing amplitude in the central cell and is strongly affected by the attractive central-cell potential. As a result, only the E and T_2 states are found at an energy given by EMT. Full calculations performed on the chalcogen donors show that the central cell gives rise to a localized state in the band gap and that it is an A_1 state mainly derived from the conduction band. In the case of single substitutional Pt, calculations show that the ground state is formed in a very different way. The d orbitals are found deep in the valence band and a vacancylike antibonding T_2 state from the valence band is pushed up into the band gap. Accordingly, there are no *a priori* reasons to expect that one of the shallow-donorlike states should substantially increase its binding energy. It is instead expected that all six donor states would still be found at an energy position close to that given by EMT.

The level ordering of the excited donor states of the T-line center is different from that observed for the shallow group-V donors and the deep chalcogen donors in silicon, for which the A_1 state has the largest binding energy, followed by the T_2 state and the E state. The E state and the T-line center is found below the T_2 state. A possible explanation of this observation is that the T_2 vacancylike state repels the excited s-like T_2 state.

In the case of the silver donor spectrum several ns lines were observed which made the assignment possible. It was found that the strongest lines belonged to the $1s$ manifold and that the intensity rapidly decreased with n for the higher s states. This indicates that the T lines are due to transitions to $1s$ donor states. The EMT binding energy of the T lines ($Z=2$) when assuming transitions to $1s$ states is about 9004 cm^{-1} and the position of the ground-state level is then inferred to be roughly 432 cm^{-1} (54 meV) above the top of the valence band.

VII. CONCLUSIONS

The T-line spectrum has been thoroughly investigated by means of perturbation spectroscopy and conclusively attributed to optical transitions to donorlike excited states from a $\Gamma_7(T_2)$ ground state. The symmetry of the center is T_d and the experimental results suggest the singly positively charged state of substitutional Pt as the chemical origin.

ACKNOWLEDGMENTS

Its a pleasure to acknowledge interesting discussions on this topic with F. Ham and G. Grossmann and their critical reading of the manuscript. Furthermore, the authors are indebted to P. Emanuelsson for his EPR work and to L. Timby and E.-L. Hellquist for help with sample preparation and to F. Anderson and G. D. Watkins for communicating their results prior to publication.

APPENDIX

In evaluating the stress and Zeeman matrices, we have chosen as basis functions simple products, $|\Gamma\mu\rangle\,|m_s\rangle$, between the orbital part $|\Gamma\mu\rangle$ and the spin part $|m_s\rangle$ and include the off-diagonal matrix elements due to the spin-orbit interaction. Γ is the irreducible representation of the orbital part, μ is the row index, and $|m_s\rangle$ are the usual spin-$\frac{1}{2}$ functions, α and β. In the matrices, the transformation properties of the T_2 states are chosen in analogy with angular momentum p functions and instead of the usual row indices (x, y, and z) we use $|T_2\mu\rangle$ with row indices 0 and ±1. $|T_2\mu\rangle$ is abbreviated as $|\mu\rangle$ and in the case of the E states, we only indicate the row indices ε and θ.

The spin-orbit matrix between $\Gamma_8(E)$ and $\Gamma_8(T_2)$ becomes

$$\begin{array}{c|cccccc} & |1\rangle\alpha & |1\rangle\beta & |0\rangle\alpha & |0\rangle\beta & |-1\rangle\alpha & |-1\rangle\beta \\ |\theta\rangle\alpha & 0 & 0 & 0 & 0 & 0 & -\xi_2 \\ |\theta\rangle\beta & \xi_2 & 0 & 0 & 0 & 0 & 0 \\ |\varepsilon\rangle\alpha & 0 & \frac{\xi_2}{\sqrt{3}} & \sqrt{\frac{2}{3}}\xi_2 & 0 & 0 & 0 \\ |\varepsilon\rangle\beta & 0 & 0 & 0 & -\sqrt{\frac{2}{3}}\xi_2 & -\frac{\xi_2}{\sqrt{3}} & 0 \end{array} \tag{A1}$$

and for the $\Gamma_8(T_2)$ manifold [omitting the diagonal elements $E(T_2)$]

$$\begin{array}{c|cccccc} & |1\rangle\alpha & |1\rangle\beta & |0\rangle\alpha & |0\rangle\beta & |-1\rangle\alpha & |-1\rangle\beta \\ |1\rangle\alpha & \frac{\xi_1}{2} & 0 & 0 & 0 & 0 & 0 \\ |1\rangle\beta & 0 & -\frac{\xi_1}{2} & \frac{\xi_1}{\sqrt{2}} & 0 & 0 & 0 \\ |0\rangle\alpha & 0 & \frac{\xi_1}{\sqrt{2}} & 0 & 0 & 0 & 0 \\ |0\rangle\beta & 0 & 0 & 0 & 0 & \frac{\xi_1}{\sqrt{2}} & 0 \\ |-1\rangle\alpha & 0 & 0 & 0 & \frac{\xi_1}{\sqrt{2}} & -\frac{\xi_1}{2} & 0 \\ |-1\rangle\beta & 0 & 0 & 0 & 0 & 0 & \frac{\xi_1}{2} \end{array} , \tag{A2}$$

where ξ_1 and ξ_2 are defined in Eq. (4).

The stress operator is diagonal in spin and the total stress matrix may be written as a 6×6 matrix. The EMT donor states are sensitive only to the hydrostatic and the E components of the stress operator and the stress operator V may be written as

$$\begin{aligned} V &= A_1 \mathrm{Tr}\sigma + E_\theta \sigma_\theta + E_\varepsilon \sigma_\varepsilon , \\ \sigma_\theta &= 2\sigma_{zz} - \sigma_{xx} - \sigma_{yy} , \\ \sigma_\varepsilon &= \sigma_{xx} - \sigma_{yy} , \end{aligned} \tag{A3}$$

where A_1, E_θ, and E_ε are electronic operators and σ_θ and σ_ε are symmetrized linear combinations of the stress tensor. We chose the stress directions to be in the plane spanned by the [001] and [110] directions which gives $\sigma_\varepsilon=0$. The stress matrix becomes

$$\begin{array}{c|cccccc} & |A_1\rangle & |\theta\rangle & |\varepsilon\rangle & |1\rangle & |0\rangle & |-1\rangle \\ |A_1\rangle & E(A_1) & \frac{\Delta\sigma_\theta}{\sqrt{2}} & 0 & 0 & 0 & 0 \\ |\theta\rangle & \frac{\Delta\sigma_\theta}{\sqrt{2}} & E(E)+\frac{\Delta\sigma_\theta}{2} & 0 & 0 & 0 & 0 \\ |\varepsilon\rangle & 0 & 0 & E(E)-\frac{\Delta\sigma_\theta}{2} & 0 & 0 & 0 \\ |1\rangle & 0 & 0 & 0 & E(T_2)-\frac{\Delta\sigma_\theta}{2} & 0 & 0 \\ |0\rangle & 0 & 0 & 0 & 0 & E(T_2)+\Delta_\theta & 0 \\ |-1\rangle & 0 & 0 & 0 & 0 & 0 & E(T_2)-\frac{\Delta\sigma_\theta}{2} \end{array} , \tag{A4}$$

where $\Delta=\Xi_u(s_{11}-s_{12})/3$ and the common diagonal elements due to the hydrostatic stress component have been omitted.

The Zeeman matrix becomes very simple, since $g_l=0$ for the donor states. Defining

$$\begin{aligned} B^1 &= -(B_x + iB_y)/\sqrt{2} , \\ B^0 &= B_z , \\ B^{-1} &= (B_x - iB_y)/\sqrt{2} , \end{aligned} \tag{A5}$$

we find that, when excluding the spin-orbit matrix elements, the Zeeman matrix has a block-diagonal form with identical 2×2 matrices

$$\begin{array}{c|cc} & |\Gamma,\mu\rangle\alpha & |\Gamma,\mu\rangle\beta \\ |\Gamma,\mu\rangle\alpha & E(\Gamma)+\mu_B B^0 & -\sqrt{2}\mu_B B^{-1} \\ |\Gamma,\mu\rangle\beta & \sqrt{2}\mu_B B^1 & E(\Gamma)-\mu_B B^0 \end{array} \tag{A6}$$

which becomes diagonal when **B** is parallel to the z direction.

[1]H. H. Woodbury and G. W. Ludwig, Phys. Rev. **126**, 466 (1962).
[2]G. D. Watkins, Physica **117&118**, 9 (1983).
[3]M. Pugnet, J. Barbolla, J. C. Brabant, F. Saint-Yves, and M. Brousseau, Phys. Status Solidi A **35**, 533 (1976).
[4]S. Braun and H. G. Grimmeiss, J. Appl. Phys. **45**, 2658 (1974).
[5]G. Armelles, J. Barrau, M. Brousseau, and J. P. Noguier Phys. Rev. B **33**, 1243 (1986).
[6]G. Armelles, J. Barrau, M. Brousseau, B. Pajot, and C. Naud, Solid State Commun. **56**, 303 (1985).
[7]M. Kleverman, J. Olajos, and H. G. Grimmeiss, Phys. Rev. B **37**, 2613 (1988).
[8]P. Omling, M. Kleverman, P. Emanuelsson, J. Olajos, and H. G. Grimmeiss, Solid State Commun. **65**, 557 (1988).
[9]R. A. Faulkner, Phys. Rev. **184**, 713 (1969).
[10]E. Janzén, R. Stedman, G. Grossmann, and H. G. Grimmeiss, Phys. Rev. B **29**, 1907 (1984).
[11]M. Kleverman, J. Olajos, and H. G. Grimmeiss, Phys. Rev. B **35**, 4093 (1987).
[12]J. Olajos, M. Kleverman, and H. G. Grimmeiss, Phys. Rev. B **38**, 2613 (1988).
[13]J. Olajos, B. Bech Nielsen, M. Kleverman, P. Omling, P. Emanuelsson, and H. G. Grimmeiss, Appl. Phys. Lett. **53**, 2507 (1988).
[14]D. K. Wilson and G. Feher, Phys. Rev. **124**, 1068 (1961).
[15]F. G. Anderson and G. D. Watkins (private communication).
[16]V. A. Singh, U. Lindefelt, and A. Zunger, Phys. Rev. B **27**, 4909 (1983).
[17]W. E. Krag, W. H. Kleiner, and H. J. Zeiger, in *Proceedings of the Tenth International Conference on the Physics of Semiconductors, Cambridge, 1970,* edited by S. P. Keller, J. C. Hensel, and F. Stern (USAEC Division of Technical Information, Washington, D.C., 1970), p. 271. Note their misprint for ξ_2.
[18]V. J. Tekippe, H. R. Chandrasekhar, P. Fisher, and A. K. Ramdas, Phys. Rev. B **6**, 2348 (1972).
[19]J. M. Luttinger and W. Kohn, Phys. Rev. **97**, 869 (1955).
[20]P. J. Dean, R. A. Faulkner, and S. Kimura, Phys. Rev. B **2**, 4062 (1970).
[21]J. S. Griffith, *The Theory of Transition Metal Ions* (Cambridge University Press, London, 1961).
[22]J. L. A. Alves and S. Larsson, J. Phys. Chem. Solids, **46**, 1207 (1985).
[23]K. Bergman, G. Grossmann, H. G. Grimmeiss, and M. Stavola, Phys. Rev. Lett. **56**, 2827 (1986).